Published in final edited form as:
Mol Cancer Res. 2018 March ; 16(3): 528–542. doi:10.1158/1541-7786.MCR-17-0272.

Nanoscale Tuning of VCAM-1 Determines VLA-4-dependent Melanoma Cell Plasticity on RGD Motifs

Katharina Amschler[#1], **Eugen Koßmann**[#1], **Luise Erpenbeck**[1], **Sebastian Kruss**[2], **Tillmann Schill**[1], **Margarete Schön**[1], **Sigrid M. C. Möckel**[1], **Joachim P. Spatz**[3], and **Michael P. Schön**[1,*]

[1]Department of Dermatology, Venereology and Allergology, University Medical Center, Göttingen, Germany

[2]Department of Physical Chemistry, Georg August University, Göttingen, Germany

[3]Department of Cellular Biophysics, Max Planck Institute for Medical Research, Heidelberg and Laboratory of Biophysical Chemistry, University of Heidelberg; Heidelberg, Germany

[#] These authors contributed equally to this work.

Abstract

The biophysical fine-tuning of cancer cell plasticity is crucial for tumor progression but remains largely enigmatic. Although Vascular Cell Adhesion Molecule-1 (VCAM-1/CD106) has been implicated in melanoma progression, here its presentation on endothelial cells was associated with diminished melanoma cell spreading. Using a specific nanoscale-modulation of VCAM-1 (tunable from 70 to 670 ligands/µm^2) next to integrin ligands (RGD motifs) in a bifunctional system, reciprocal regulation of integrin α4 (ITGA4/VLA-4/CD49d)-dependent adhesion and spreading of melanoma cells was found. As the VCAM-1/VLA-4 receptor pair facilitated adhesion, while at the same time antagonizing RGD-mediated spreading, melanoma cell morphogenesis on these bifunctional matrices was directly regulated by VCAM-1 in a dichotomic and density-dependent fashion. This was accompanied by concordant regulation of F-actin cytoskeleton remodeling, Rac1-expression and paxillin-related adhesion formation. The novel function of VCAM-1 was corroborated *in vivo* using two murine models of pulmonary metastasis. The regulation of melanoma cell plasticity by VCAM-1 highlights the complex regulation of tumor-matrix interactions.

Implications—Nanotechnology has revealed a novel dichotomic function of the VCAM-1/ VLA-4 interaction on melanoma cell plasticity, as nanoscale tuning of this interaction reciprocally determines adhesion and spreading in a ligand density-dependent manner.

Introduction

Notwithstanding recent advances in the treatment of melanoma, this aggressive skin tumor is fatal in most cases once distant metastases occur (1–5). The formation of metastases depends on extravasation of tumor cells from blood or lymph vessels, a complex process that

[*]correspondence: Michael P. Schön, Department of Dermatology, Venereology and Allergology, University Medical Center Göttingen, Robert-Koch-Str. 40, 37075 Göttingen, Germany, phone: +49-551-3966401, michael.schoen(at)med.uni-goettingen.de.

Europe PMC Funders Author Manuscripts

Europe PMC Funders Author Manuscripts

is orchestrated by a plethora of accessory cells, soluble and sessile mediators as well as nanoscale adhesive interactions (6).

VCAM-1 (Vascular Cell Adhesion Molecule-1, CD106) was one of the first adhesion molecules implicated in metastasis-promoting endothelial cell interactions with malignant tumors, including melanoma (7–10). Indeed, it has been a paradigm for 25 years now that endothelial expression of VCAM-1 facilitates melanoma progression and metastasis through binding to its predominant receptor, VLA-4 (Very Late Antigen-4, $\alpha_4\beta_1$ integrin, CD29/CD49d) on melanoma cells (11–14). Evidence for this notion came from both murine (12,15) and human studies, with the latter linking VCAM-mediated interactions with expression of its ligand, VLA-4, and „aggressiveness" of the tumor cells (16). However, emerging evidence suggests a more complex and versatile role of VCAM-1/VLA-4 interactions, at least in certain tumors (17), a notion that is supported by a recent study showing that strong up-regulation of VCAM-1 on pulmonary microvessels did not lead to increased experimental melanoma metastasis *in vivo* (18).

A number of influencing factors have been implicated in the focal regulation of VCAM-1 expression *in vivo*. These include shear stress on the vessel wall (19–22), tumor cell and immune cell-produced cytokines and chemokines (23) as well as direct or indirect contact of tumor cells with the endothelial lining (24–26). Under certain experimental conditions, melanoma cells may stimulate expression of VCAM-1 directly at pulmonary metastatic sites (24). In addition to up-regulation during inflammation or metastasis, VCAM-1 can undergo ectodomain shedding leading to a net reduction of its density (27,28).

As density, clustering or neighborhood relation of cell surface molecules can hardly be determined precisely on the nanoscale under *in vivo* or conventional *in vitro* conditions such as random coating of plastic tissue culture ware, the exact biophysical composition and consecutive functional relevance of VCAM-1- or VLA-4-containing microdomains still remain unknown. Currently available model systems do not allow the study of isolated VCAM-1 functions, let alone VCAM-1 functions in conjunction with other adhesion receptors in bifunctional systems, with exact and measurable adjustment of biophysical properties. As a consequence of this less-than-optimal situation, the role of VCAM-1 for the dynamics and morphogenesis of malignant cells cannot be understood.

Based on nanopatterning and biofunctionalization concepts, we now provide experimental evidence for an unexpected dichotomic function of VCAM-1 towards human melanoma cells. Experimental platforms modeling density variation of relevant receptors and extracellular signals in a nanoscopically defined spatial arrangement allow the study of functional consequences of important (patho)physiological regulations such as receptor distribution. Therefore, such nanotechnological approaches can refine our models of tumor cell biology. To mimic the variable presentation of VCAM-1, we have generated mono- and bifunctional matrices based on gold nanopatterns functionalized with VCAM-1 alone or interspersed with RGD binding motifs, respectively. These nanoscopically defined matrices are models of endothelial cell surfaces in different states of activation. VCAM-1 site densities were tunable over one order of magnitude (from 70 ligand sites/μm^2 to 670 ligand sites/μm^2). We demonstrate that nanoscopic VCAM-1 mediates firm attachment of melanoma cells but, unexpectedly, simultaneously inhibits RGD-induced melanoma cell spreading as well as the associated cytoskeletal reorganization and focal contact formation in a density-dependent fashion. These results may shift the paradigm of a unidirectional function of VCAM-1 by demonstrating that its interaction with VLA-4 can elicit a seemingly paradoxical inhibition of melanoma cell spreading. The inhibitory activity was specific for the VCAM-1/VLA-4 interaction. Thus, our results indicate a new, density-dependent function of VCAM-1 towards melanoma cells with implications for the fine-tuning of integrin-mediated spreading.

Materials and Methods

Cell culture and preparation for functional experiments

The human melanoma cell lines A375 and MeWo as well as the murine melanoma line B16F10 were grown in Dulbecco's Modified Eagle's Medium (DMEM) supplemented with 10% fetal calf serum (FCS), 2 mM L-glutamine, 100 units/ml penicillin, 100 µg/ml streptomycin (all from Invitrogen, Darmstadt, Germany), at 37°C in a humidified 5% CO_2 atmosphere. Culture medium and solutions were pre-warmed before use. Cells were sub-cultured twice a week using trypsin (0.05% w/v)/EDTA (5 mM) for detachment. All cells were easily recognizable as melanoma cells by their melanin production. Sources (ATCC, catalogue no. CRL-1619), identity and routine mycoplasma testing of the cells have been described previously (29). Cells were expanded and multiple aliquots were stored frozen. Cells used for experiments were not passaged more than five times. PCR testing for mycoplasma contamination was performed on a routine basis according to the manufacturer's instructions (Biontex, München, Germany), and cells used for experiments were negative for mycoplasma.

Functional experiments with human melanoma cells were performed in six-well culture plates (Greiner bio-one, Frickenhausen, Germany). The cells were harvested at a confluence of ≈70% using 1 ml Accutase Solution (PromoCell, Heidelberg, Germany) for 5 min at 37°C. Cells were then re-suspended in complete DMEM and counted. After washing with PBS and re-suspension in DMEM containing 10% FCS, the cells were placed in the incubator for 20 min before being added to the functionalized matrices at a final concentration of 10^5 cells per ml. After incubation for 30 - 45 minutes at 37°C, the matrices with adherent cells were washed with PBS for 5 minutes. To ascertain the validity of the results with short adhesion periods, the experiments were repeated with observation periods of up to 3 h. Phase-contrast images from random positions were taken at different time points using an Axiovert 200 system (Zeiss, Göttingen, Germany).

Melanoma cell adhesion on endothelial cells

Human umbilical vein endothelial cells (HUVEC; Lonza, Basel, Switzerland) were cultured in endothelial cell growth medium (EGM; Lonza) supplemented with gentamycin at 37°C and 5% CO_2 in a humidified atmosphere. HUVEC were used at passages four to six. Upon confluence, endothelial cells were exposed for 4 h to recombinant human TNFα (25 ng/ml; ImmunoTools, Friesoythe, Germany). Binding sites of VCAM-1 were blocked for 1 h using a function-blocking VCAM-1-directed antibody, or the cultures were exposed to an equal

Europe PMC Funders Author Manuscripts

amount of an unrelated isotype-matched control antibody. PKH26 (Sigma, Deisenhofen, Germany)-labeled human melanoma cells (10^5) were allowed to attach for 40 min. Wells were washed three times in a standardized manner with PBS. Adhesion and spreading were documented using an inverted fluorescence microscope (Zeiss, Axiovert 200) and quantitated using ImageJ (http://rsb.info.nih.gov/ij/).

Nanopatterning

Nanostructured matrices were produced by block copolymer micellar nanolithography (BCML) (30–33). In short, glass cover slides (24 x 24, No. 1; Carl Roth, Karlsruhe, Germany) were cleaned in caroic acid (1 h, 1:3 H_2O_2 (30%): H_2SO_4 (p.A., Merck, Darmstadt, Germany). These glass slides were then sonicated four times for 5 min each and dried with N_2. Micellar solutions were prepared in a Glove Box (Braun, Garching, Germany) by dissolving the polystyrene-polyvinylpyridine-block-copolymers (Polysciences, Warrington, FL, USA) in toluene (Merck). The micelles' cores were then loaded with $HAuCl_4 \cdot 3H_2O$ (Sigma). The cleaned glass cover slips were dip coated into the micelle solution in a standardized fashion. Organic parts of the micelles were removed by plasma treatment (10% H_2, 90% Argon, 0.4 mbar, 150 W, TePla 100; PVA, Wettenberg, Germany). Gold nanoparticles, herein referred to as Au-NP, were thus firmly bound to the glass surface.

Nanoscopically defined matrices were generated with a wide range of Au-NP spacings (mean distances between adjacent nanoparticle sites). The actual densities of each batch of nano-matrices were determined precisely by scanning electron microscopy (Ultra 55; Zeiss) and covered the range from 70/μm^2 to 670/μm^2 (corresponding to ligand site distances ranging from 40 nm to 120 nm). As micellar block copolymer nanolithography results in a quasi-hexagonal assembly of the nanoparticles, hence the ligand site density can also be approximated by applying the formula $x = 2/(d2\sqrt{3})$.

Biofunctionalization

Biofunctionalization was performed in 60 mm Petri dishes (Greiner). Nanostructured glass surfaces were UV-ozone-cleaned (UV-Ozone Cleaning System UVOH 150 LAB; FHR Anlagenbau, Ottendorf-Okrilla, Germany) for 10 min (0.8 slm). Afterwards, matrices were incubated with 100 μl of 0.5 mg/ml PLL(20kDa)-g-[3.5]-PEG(2kDa) and PLL(20kDa)-g-[3.5]-PEG(2kDa)/PEG-RGD(3.4kDa) (SuSoS, Dübendorf, Switzerland), respectively, and 10 mM HEPES (4-(2-hydroxyethyl)-1-piperazineethanesulfonic acid; Calbiochem, Bad Soden am Taunus, Germany) at pH 7.4 for 45 min on parafilm. Then, the matrices were washed in *aqua dest*. for 30 min and were carefully dried. Thereafter, they were incubated with 200 μl of 1 mg/ml HS-(CH2)11-EG3–NTA (NTA=nitrilotriacetic acid; Prochimia, Sopot, Poland) in ethanol solution (1:5) for 90 min. Ni^{2+} was bound to the NTA-group by incubating the matrices for 20 min with 120 μl of a 10 mM $NiCl_2$ (Merck) solution in HBS (10 mM HEPES, 75 mM NaCl; Carl Roth) at pH 7.5. Finally, the matrices were incubated with 10 μg/ml VCAM-1 (VCAM-1 recombinant protein His tagged, HEK293-derived, MyBioSource, San Diego, CA, USA) or PECAM-1 (PECAM-1 recombinant protein, His tagged, HEK293-derived, MyBioSource), respectively, in PBS for 2.5 h. It had been established in additional adhesion experiments that His-tagged and non-His-tagged VCAM-1 exerted identical activities towards adhesion and spreading of human melanoma cells (cell lines A375 and MeWo). After biomolecule functionalization, the matrices were washed with PBS for 15 min before being used in cell experiments. Matrices were generally equilibrated in the corresponding solvent before and washed with the corresponding solvent for 10 min after each functionalization step. It had been established by adhesion experiments with A375 melanoma cells that treatment with NE did not reduce the passivating capacity of the PEG coating.

Surface characterization

Quartz crystal microbalance with dissipation (QCM-D) is an electromechanical method measuring frequency changes of (coated) oscillating quartz crystals. Such frequency changes can provide information about adsorption processes taking place on the coated surface. For QCM-D measurements, an E4 System (Q-Sense, Stockholm, Sweden) was used. Gold-coated quartz crystals (4.95 MHz, Q-Sense) were cleaned for 45 min/150 W in O_2-plasma (TePla 100). The same molecules and solvents were used for surface characterization and biofunctionalization.

In order to prove successful biomolecule binding to the Au-NPs, functionalized matrices were incubated with 10 µg/ml of mouse anti-human VCAM-1 IgG1 antibody (clone 1.G11B1; LifeSpan BioSciences, Seattle, WA, USA) for 2 h. After further incubation with 8 µg/ml of a second fluorescein-labeled anti-mouse antibody (Cell Signalling Technology, Boston, MA, USA) for 1 h, the margin of functionalization was detected with fluorescence microscopy (Axiovert 200; Zeiss)

siRNA transfection of human melanoma cells

The siRNA directed against the human integrin subunit α_4 (Hs_ITGA4_6; Qiagen, Hilden, Germany) as well as the non-targeting control siRNA (AllStars Neg. Control siRNA; Qiagen) were diluted according to the manufacturer's instructions and stored at -20°C. Melanoma cells were transfected with siRNA at a concentration of 125 nM using the Lipofectamine 2000 reagent (Invitrogen) according to the manufacturer's instructions. Cells were added to the siRNA–lipofectamine suspension and DMEM without antibiotics. The transfection was repeated after 24 h of incubation. Transfected cells were harvested after a further incubation of 72 h and directly used in experiments with parallel flow cytometry analysis of α_4-integrin expression.

Flow cytometry

Melanoma cells (in their exponential growth phase) were harvested using Accutase (PromoCell), washed with PBS, resuspended in PBS containing 5% human male AB-serum (Sigma), and incubated with 1 µg/ml of either anti-α_4 (clone P1H4, Abcam, Cambridge, England), anti-$\alpha_V\beta_3$ (clone LM609, Merck), anti-α_5 (clone SAM-1, Beckman-Coulter, Brea, CA, USA), anti-β_1 (clone 4B4LDC9LDH8, Beckman-Coulter) or an IgG1 isotype control (Zymed, Wien, Austria). Surface-bound primary antibodies were detected using 0.5 µl of Alexa Fluor 488-conjugated goat-derived anti-mouse IgG (H+L) as a secondary reagent (Cell Signalling Technology). Analysis was performed using the FACS Canto II and the FACS Diva software (BD biosciences, Heidelberg, Germany).

Europe PMC Funders Author Manuscripts

Europe PMC Funders Author Manuscripts

Cleavage of VCAM-1 by neutrophil elastase (NE)

Human Neutrophil Elastase (Elastin Products, Owensville, MO, USA) was diluted in PBS at a stock concentration of 100 µg/ml. Biofunctionalized VCAM-1-matrices were incubated with 10 µg/ml of human neutrophil elastase dissolved in 100 µl PBS for 30 min at 37°C. Control matrices were incubated with 100 µl PBS. Subsequently, both matrices were washed twice in PBS prior to their use in experiments.

Immunofluorescence Assays and microscopy

Matrices were washed in PBS and attached cells were fixed with 4% formaldehyde/PBS for 30 min at room temperature. Subsequently, the samples were blocked with 5% FCS in PBS for 60 min followed by anti-paxillin (clone Y133, Abcam) for 3 h at room temperature. After 3 washing steps in PBS, cells were incubated with Alexa Fluor 488-conjugated anti-mouse IgG F(ab')2 (Cell Signaling) for 1 h. F-actin was then stained with phalloidin (PromoFluor-55; PromoCell) for 30 min. Fluorescence Mounting Medium (Dako, Hamburg, Germany) containing 0.5 µg/ml DAPI (Sigma) resulted in nuclear staining. Fluorescence microscopy was performed on an Axio Imager M.1 system equipped with an AxioCam MRm (Zeiss).

Polymerase chain reaction

Total RNA was extracted using the Rneasy Mini Kit (Qiagen) according to the manufacturer's instructions. Two µg of total RNA were transcribed using First Strand cDNA-Synthesis Kit (Fermentas, St. Leon-Rot, Germany). For DNA amplification, Taq-DNA-Polymerase (PeqLab, Erlangen, Germany) was used. Primers and conditions used are detailed in the Supplementary online material (Supplemental Table 1).

Data analysis

After defined time intervals (specified in the results section), standardized overview-photomicrographs were analyzed morphometrically using ImageJ. For measurement of cell areas, a grid (220x290 µm) was set on the image center of a 16x field. All cells within this grid were accepted for measurement granting a standardized and randomized analysis.

For the analysis of focal adhesions, images of cells stained with with phalloidin and a paxillin-directed antibody were split into different color channels via ImageJ. Within the green (paxillin stain) channel the threshold of brightness and contrast was adjusted individually for every cell in order to distinguish between circumferential focal adhesions and background signals. Particles between 0.1-5 μm^2 (this range includes the cut-off-value of 2 μm^2 which distinguishes between mature and immature focal adhesions) (34) were considered as focal adhesions and counted using ImageJ. The method was confirmed by manual counting and manual size measurements of focal adhesions showing similar results.

GFP transfection of melanoma cells and short-term pulmonary metastasis in mice

Green fluorescent protein (GFP) was stably transfected into B16F10 melanoma cells according to an optimized protocol using 1.5×10^6 cells, 2 µg, and 100 µl of Nucleofector solution V (Amaxa, Cologne, Germany). Transfected cells expressing high levels of GFP were subcloned thrice, selected in DMEM (Invitrogen) supplemented with 1 mg ml^{-1} of G418 selection compound (Sigma) and sorted by fluorescence-activated cell sorting. In general, 10^6 GFP-labelled melanoma cells were injected *via* the lateral tail vein. Mice were sacrificed 1 min, 5 min or 30 min after tumor cell injection (n=3 mice in each group), and the lungs were immediately snap-frozen in liquid nitrogen. Two complementary lines of experiments were performed to achieve different expression states of VCAM-1 in pulmonary capillaries: The animals were either untreated or received an intra-tracheal instillation of 0.5 µg of the TLR2/6 agonist, MALP-2 (Macrophage-activating lipopeptide-2), 24 h prior to tumor cell injection as described (18). Cryostat-cut sections of the lungs were assessed by double fluorescence analysis (with GFP identifying melanoma cells and phycoerythrin-labeled antibodies detecting VCAM-1). Animal experiments were approved by the appropriate governmental authority (LAVES, permission number 33.9-42502-04-14).

Statistical analysis

Data represent means ±SEM of at least three independent experiments. One-way ANOVA test was performed to detect differences between the four estimated VCAM-1 densities of 670, 280, 120 and 70 proteins per μm^2. After confirming normal distribution of the data points, further individual comparisons between two matrices were performed by the Student's two-tailed, unpaired t-test. Means determined to be significantly different ($p<0.05$) were subjected to post hoc tests using Bonferroni's correction analysis.

Results

Inhibition of VCAM-1 facilitates melanoma cell spreading on activated endothelial cells

Since the consequences of endothelial cell expression of VCAM-1 for cancer cell functions have not been explored in detail, we were initially interested in direct functional activities of VCAM-1 in the interaction with human melanoma cells. Towards this end, human endothelial cells were exposed to TNFα (25 ng/ml) to stimulate a robust expression of VCAM-1 (Figure 1a) (35).

Melanoma cell adhesion was not affected by antibody-mediated inhibition of VCAM-1 (isotype, 29.3 (±6.9) cells/0.1 mm^2, vs. anti-VCAM-1, 33.3 (±7.1) cells/0.1 mm^2, difference not significant; Figure 1b and 1c, left graph), presumably due to compensation by other endothelial adhesion molecules induced by TNFα. However, we observed a striking and hitherto unknown morphological effect inasmuch as a conspicuously higher number of melanoma cells spread on the endothelial layer when VCAM-1 had been blocked (Figure 1b and 1c, right graph): While endothelial cell cultures treated with an isotype-matched control antibody facilitated spreading of 17.2 (±5.1) A375 melanoma cells/ 0.1 mm^2, exposure to a function-blocking antibody directed against VCAM-1 resulted in spreading of 27.0 (±5.7) melanoma cells/ 0.1 mm^2 (p=0.00034). In contrast, melanoma cells that firmly adhered but did not spread were 12.0 (±5.1) / 0.1 mm^2 on isotype-treated but only 6.3 (±2.7) / 0.1 mm^2 on anti-VCAM-1-treated endothelial cells (p=0.00351). In addition, spread melanoma cells were significantly larger by 13% when VCAM-1 was blocked (based on individual morphometric measurements of 392 cells on control cultures and 356 cells on cultures with

VCAM-1-inhibition; p=0.001). These significant VCAM-1 function-associated differences of melanoma cell behavior were not discernable from previous data and opened up the possibility of a dichotomic function of VCAM-1 for static melanoma cell adhesion on the one hand and spreading on the other.

Given that the molecular elucidation of this intriguing dichotomy was not possible by conventional methods, we have devised and utilized a tunable nanotechnology-based experimental system to investigate the unexpected traits of VCAM-1 on the nanoscale.

Defined VCAM-1 nanoscale patterns specifically support melanoma cell adhesion

Matrices presenting different site densities of VCAM-1 were created by combining nanopatterning and subsequent biofunctionalization. We used block copolymer micellar nanolithography (BCML) as a platform to control lateral distribution and density of gold-nanoparticles (Au-NP) (30,31,36). Each Au-NP ideally serves as an anchor point for a single VCAM-1-molecule which is covalently bound in a site-directed manner using subsequent steps of biofunctionalization: In the first step, glass slides were covered with Au-NPs using BCML (Figure 2a shows an example of a nanopatterned glass substrate with 6 nm-Au-NP-dots). For this study, we created different distances from 40 to 120 nm, corresponding to ligand site densities ranging from 670/μm^2 to 70/μm^2, i.e. covering one order of magnitude. Next, we covalently bound HS-(CH2)11-EG3-NTA to the Au-NPs using nitrilotriacetic acid (NTA) head groups and $NiCl_2$ for site-directed immobilization of human recombinant His-tagged VCAM-1 (Figure 2b). In order to control for successful bio-functionalization, we performed Quartz Crystal Microbalance with Dissipation (QCMD) monitoring on homogeneous gold, demonstrating that VCAM-1 was bound correctly to gold through its terminal His6-sequence, thus mimicking the physiological orientation of a transmembrane type I protein (Figure 2c). Passivation (PLL-g-PEG) in-between the Au-NPs prevented nonspecific binding of cells or proteins. The margin of functionalization on the slides provided an internal control for both the functional presentation of VCAM-1 and the passivation, as immunofluorescence microscopy demonstrated binding of VCAM-1-directed antibodies exclusively to the nano-patterned areas. Because of the passivation layer between the Au-NPs, neither VCAM-1 nor VCAM-1-directed antibodies adsorbed to areas without Au-NPs (Figure 2d, left panel). When two human melanoma cell lines (A375 and MeWo) were incubated with a VCAM-1-functionalized surface, cells did not adhere beyond the margin of functionalization, again showing the low nonspecific background of our model system (Figure 2d, right panel).

Nanoscale VCAM-1 presentation facilitates attachment but not spreading of melanoma cells

Two human melanoma cell lines (A375 and MeWo) expressing the dimeric $\alpha_4\beta_1$ integrin (VLA-4, CD29/CD49d) at high levels (i.e., MFI>2,000) bound firmly to nanoscopic VCAM-1 matrices in a strictly density-dependent fashion (Figure 2e, f) but, surprisingly, did not spread on this ligand (Figure 2g, left panel). In striking contrast, a matrix with 10%-15% RGD (arginine-glycine-aspartic acid) motifs interspersed within the pegylation areas readily facilitated profound melanoma cell spreading (Figure 2g, middle panel). RGD is known to induce spreading *via* integrin-activation (37), with the linear form used here binding preferentially to the $\alpha_5\beta_1$ and $\alpha_V\beta_3$ integrins, respectively (38). However, when both integrin-directed signals (RGD and VCAM-1) were combined within the same matrix, melanoma cells adopted an intermediate phenotype (Figure 2a, right panel). Human melanoma cells showed strong expression of all integrins implicated in the interaction with VCAM-1 and RGD, respectively (Figure 2h).

To better understand these apparently distinct and opposite integrin-mediated functions in human melanoma cells, the following experiments were designed to analyze different site densities of VCAM-1 in bifunctional association with the RGD-peptide as a second signal presented within the pegylation areas.

Tuning of VCAM-1-densities in bifunctional matrices controls melanoma cell behavior

When human melanoma cells were exposed to bifunctional matrices displaying RGD in combination with nanostructured VCAM-1 at varying and tunable densities, it became apparent that RGD-mediated spreading could be precisely down-modulated by the VLA-4-directed activity of VCAM-1. This function was density-dependent in a manner reciprocal to the VLA-4/VCAM-1-mediated attachment:

As expected, control matrices (RGD alone) enabled full spreading of human melanoma cells (37). However, tuning VCAM-1 to higher densities linearly inhibited cell spreading (Figure 3a), while adhesion was not affected (Figure 3b). When the cell surface areas were measured, VCAM-1-presentation at 70 ligand sites per μm^2 (standardized ligand site distance 120 nm) did not modify cell spreading, whereas 120 ligand sites per μm^2 (distance 90 nm) reduced the cell sizes moderately to 80.69% of the controls (SD ±13%, not statistically significant). Higher densities, however, significantly reduced cell spreading: At 280 ligand sites per μm^2 (distance 65 nm), we saw a reduction to 66.54% (SD ±16.88%; p=0.02), and 670 ligand sites per μm^2 (distance 40 nm) decreased the cell sizes to 48.30% (SD ±0.09%; p=0.0001; Figure 3c). Confirming that these results hold true in general, similar results were obtained with a second unrelated melanoma cell line (MeWo). Again, VCAM-1 at a density of 70 ligand sites per μm^2 (distance 120 nm) did not affect cell spreading compared to presentation of RGD alone, whereas higher densities of VCAM-1 gradually inhibited cell spreading with 670 ligand sites per μm^2 (distance 40 nm) significantly reducing the cell size to 60.42% (SD ±18.34; p=0.037; Figure 3a, bottom row, and supplemental Figure 1). No further spreading was observed with longer observation times of up to 3 h.

These results suggested that i) VCAM-1 exerted an unexpected inhibitory function on RGD-mediated melanoma cell spreading when displayed at intermediate (280 ligand sites/μm^2) to high (670 ligand sites/μm^2) densities, ii) that numeric variations of VCAM-1-densities governed this function in a unidirectional linear fashion and iii) that this novel function was exerted independently of or in addition to the adhesive function. The following experiments were designed to dissect and confirm this intriguing finding in more detail, because morphologic changes of tumor cells may affect a number of important functions such as migration, invasion (including extravasation as a particular form of invasion) and metastasis.

Europe PMC Funders Author Manuscripts

Europe PMC Funders Author Manuscripts

VCAM-1-density variation controls dichotomous features in paxillin-related adhesion formation

To understand the VCAM-1-dependent inhibition of cell spreading mechanistically, F-actin (a parameter for cytoskeletal re-organization) and paxillin (a focal adhesion marker specifically binding to the α_4 integrin) (39) were visualized in human melanoma cells (A375 and MeWo). Indeed, the formation of paxillin-related adhesions (defined to measure 0.1 μm^2 to 5 μm^2) was strongly dependent on VCAM-1-density: In line with the inhibition of cell spreading, F-actin accumulation was markedly reduced on high VCAM-1 densities, whereas densities of less than 280/μm^2 facilitated stress fiber formation (Figure 3d, upper panel). In addition, intermediate to high VCAM-1 densities (280 ligand sites/μm^2 - 670 ligand sites/μm^2) showed a clearly reduced number of paxillin-related focal adhesions, which were significantly larger compared to low densities of VCAM-1 (70 ligand sites/μm^2 - 120 ligand sites/μm^2). In contrast, low densities of VCAM-1 induced significantly more but smaller paxillin-related adhesions (Figure 3d, lower panel). In detail, a low VCAM-1-density of 70 ligand sites per μm^2 induced 32.82 (SD±5.68) focal adhesions per cell with an average size of 0.57 μm^2 (SD ±0.1 μm^2) and a VCAM-1 density of 120 ligand sites/μm^2 induced 25.55 (SD ±4.73) focal adhesions per cell with a size of 0.65 μm^2 (SD ±0.02 μm^2). A ligand site density of 280/μm^2 induced 22.66 (SD ±8.36) focal adhesions with a size of 0.73 μm^2 (SD ±0.07 μm^2), which was significantly larger compared to the size of focal adhesions on matrices with 120 ligand sites per μm^2 (p=0.0370). Finally, a very high VCAM-1 density of 670 sites/μm^2 resulted in only 8.29 (SD ±1.39) focal adhesions per cell with an average size of 0.91 μm^2 (SD ±0.12 μm^2), thus being significantly fewer and larger compared to focal adhesions on matrices with 120 or 70 ligand sites per μm^2, respectively (p=0.0111 and p=0.0201, respectively; Figure 3d, e). The reduced number of paxillin-related adhesions per cell correlated directly with increasing VCAM-1 density (p=0.0441 comparing 670 ligand sites/μm^2 with 280 ligand sites/μm^2, p=0.0013 comparing 670 ligand sites/μm^2 with 120 ligand sites/μm^2, and p=0.0005 comparing 670 ligand sites/μm^2 with 70 ligand sites/μm^2, respectively; Figure 3d, f). Thus, intermediate to high VCAM-1 densities (280 ligand sites/μm^2 - 670 ligand sites/μm^2) did not support stress fiber formation, which was accompanied by very few but significantly larger paxillin-related adhesions. In contrast, low VCAM-1 densities (70 ligand sites/μm^2 – 120 ligand sites/μm^2) permitted F-actin accumulation associated with a high number of small paxillin-related adhesions.

VCAM-1 density is associated with Rac-1 expression in human melanoma cells

Further mechanistic insight into the VCAM-1-dependent regulation of melanoma cell spreading was obtained by analyzing the transcription of tumor progression-related genes in melanoma cells interacting with bifunctional matrices with high or low VCAM-1 densities (670 vs. 70 ligand sites/μm^2, respectively): The two GTPases, RhoA and Rac-1, are involved in the cytoskeletal organization (40), whereas cyclin D1 and Cdc25 are players in the mitotic machinery (41). While the expression of RhoA, cyclin D1 and Cdc25c was similar under both conditions, the expression of Rac-1 was higher by 41.9% at 70 compared to 670 VCAM-1 sites/μm^2 (p=0.013; Figure 3g, h). Given that Rac-1 is an important regulator of lamellipodia formation (40), its isolated down-regulation on high VCAM-1 densities correlated conspicuously with the inhibitory effect of VCAM-1 on spreading.

Europe PMC Funders Author Manuscripts

The regulation of melanoma cell morphogenesis is specific for the interaction of nanoscopically presented VCAM-1 with VLA-4 on melanoma cells

Three series of complementary control experiments were conducted to confirm that the regulation of melanoma cell spreading behavior was specific for VCAM-1 interacting with VLA-4 on melanoma cells:

First, VCAM-1 was cleaved off the bifunctional nanostructured matrices by neutrophil elastase (NE), which degrades VCAM-1 (27,28). It was established first that NE influenced neither the passivating pegylation nor the function of RGD interspersed within the pegylated surface (data not shown). Indeed, when matrices functionalized with VCAM-1 (280 ligand sites/μm^2) were incubated with NE for 20 minutes, human melanoma cells were not significantly impaired in their RGD-mediated spreading behavior, which was in clear contrast to matrices with uncleaved VCAM-1 (the size of cells on uncleaved VCAM-1 matrices reached 60.31% (±14.97%) of cell sizes on RGD-only matrices (p=0.0001), while the size of cells on NE-cleaved matrices was 89.35% (±9.52%; not significant; Figure 4a, b)). Thus, enzymatic cleavage of VCAM-1 abrogated its regulatory effect on melanoma cell spreading.

Second, we replaced VCAM-1 with Platelet Endothelial Cell Adhesion Molecule-1 (PECAM-1, CD31), a related immunoglobulin superfamily ligand, which is similar in size. Successful functionalization was controlled using a PECAM-1-directed antibody to visualize the margin of functionalization (not shown). When PECAM-1- and VCAM-1-functionalized nanosurfaces, respectively, were incubated with melanoma cells, only VCAM-1 but not PECAM-1 inhibited RGD-induced cell spreading. Melanoma cells on VCAM-1 matrices (280 ligand sites/μm^2) reached only the above-mentioned 60.31% (±14.97%) of the size of cells on RGD-only matrices (p=0.0001), while cells on PECAM-1 matrices (280 ligand sites/μm^2) reached 100.74% (±29.36%, p=0.0040) compared to VCAM-1-containing bifunctional matrices (Figure 4a, b). These results indicate that a related adhesion molecule could not exert the regulatory function found for VCAM-1.

Third, we down-regulated the major interaction partner of VCAM-1, the α_4 integrin (VLA-4, CD49d), on melanoma cells by siRNA-based knock-down. While untreated melanoma cells as well as melanoma cells transfected with control siRNA constructs showed high expression of α_4 (MFI=2,195.24, ±311.21), cells transfected with anti-α_4-siRNA showed a significantly reduced expression of α_4 (MFI=1,087.75, ±270.25; reduction by 50.45%; p=0.0017; Figure 4c, d). Other integrins potentially relevant in our system, i.e. α_5, β_1 and $\alpha_V\beta_3$, respectively, showed no alteration following α_4 knock-down (data not shown). When the respective cells were incubated with nanostructured VCAM-1-presenting matrices (280 ligand sites/μm^2), the control siRNA-transfected cells reached a cell size of 56.09% (±11.30%) compared to cells on RGD-only matrices. In contrast, down-regulation of the α_4 integrin subunit resulted in a cell size of 87.18% (±18.35%) relative to the RGD-only controls (p=0.0278 for control siRNA transfected cells *versus* α_4-directed siRNA knock-down cells; Figure 4e, f). Corresponding immunofluorescence analysis showed a rescue of F-actin accumulation in melanoma cells with reduced α_4-expression on VCAM-1-matrices, in contrast to the control-transfected cells (Figure 4e). Thus, the VCAM-1-

mediated inhibition of melanoma cell spreading on RGD matrices depended on expression of the α_4 integrin.

Contact with VCAM-1 expressed by pulmonary blood vessels is associated with globular morphology of melanoma cells *in vivo*

The next series of experiments was designed to address the *in vivo* relevance of the results of our nanotechnology-based *in vitro* experiments. Previous studies have demonstrated that blocking of VCAM-1 can diminish long-term experimental pulmonary melanoma metastasis (12,15). To refine the aspect of VCAM-1 in very early steps of metastasis, we have established and utilized two complementary modified mouse models to address the association of circulating melanoma cells with VCAM-1-expressing endothelia *in vivo*. Because previous models addressing the role of VCAM-1 for melanoma metastasis have entailed inflammation (thus making the assessment of VCAM's role difficult), we have used one experimental setting without and another with a pulmonary inflammatory response. In the first setting, C57BL6/J mice were not pre-treated, while in a complimentary setting VCAM-1 expression on pulmonary capillary vessels was induced by intra-tracheal instillation of the TLR2/6 ligand, MALP-2. Syngeneic B16F10 murine melanoma cells strongly expressing VLA-4 (the major ligand of VCAM-1; Figure 5a) were stably transfected with green fluorescent protein (GFP) and injected intravenously into syngeneic C57BL6/J mice. The lungs were analyzed after 1, 5 and 30 min (n=3 mice in each group) by fluorescence microscopy.

As expected (18), pre-treatment with MALP-2 led to a significant 2.3-fold increase of the density of VCAM-1-expressing pulmonary blood vessels (3.65 (±0.69) vs. 8.39 (±1.73) vessels per 20x-microscopic field; n=41 fields in each group; $p<0.0001$; Figure 5b, left graph). The numbers of melanoma cells within the lungs were similar after all three time points, and the numbers of GFP-expressing B16F10 melanoma cells were similar in untreated mice and in mice pre-treated with MALP-2 (4.02 (±1.39) cells per 20x-microscopic field vs. 3.61 cells (±1.00); n=41 fields in each group; Figure 5b, middle graph).

Surprisingly however, while similar proportions of melanoma cells were found in direct contact with pulmonary endothelial cells (7.89% in untreated vs. 7.42% in MALP-2-treated mice; Figure 5b, right graph), in both models virtually all melanoma cells contacting VCAM-1 *in vivo* appeared small and round-shaped. In contrast, all other melanoma cells within the pulmonary parenchyma or contacting VCAM-1-negative endothelia were larger and of dendritic morphology (Figure 5c), thus corroborating our *in vitro* results showing inhibition of melanoma cell spreading by VCAM-1.

Discussion

The use of nanotechnology was essential for unraveling a hitherto unknown "dichotomic" function of VCAM-1 (Figure 6), a long-known endothelial adhesion molecule implicated in tumor metastasis. First hints for this novel dichotomy, however, stemmed from our observations that inhibition of VCAM-1 facilitated spreading of melanoma cells on activated endothelial cells *in vitro*. This finding has been underscored in short-term experimental metastasis experiments *in vivo*, where stable expression of a fluorescent protein revealed that melanoma cells adjacent to VCAM-1-expressing pulmonary capillaries adopted a globular shape. Until now, the tumor-promoting effect of VCAM-1 has been attributed primarily to its adhesive function (11,26), which is thought to enhance intra-vascular arrest of circulating tumor cells and, consequently, metastasis into distant organs (42–44). It is thought that tumor cells become physically entrapped and simultaneously interact with endothelial ligands in capillaries of metastatic end-organs prior to initiating the next steps of metastasis formation (45). However, our work now provides evidence that besides adhesion, VCAM-1 mediates a prolonged and density-dependent inhibition of melanoma cell spreading. Thus, the heterogeneous nanoscale decoration of VCAM-1 within the microvessels is likely a part of a regulatory network governing tumor cell adhesion on the one hand and spreading on tissue surfaces on the other (Figure 6). Our findings might, therefore, shift the paradigm of the pathophysiological function of VCAM-1 in melanoma progression. However, the net (patho)physiological consequences of VCAM-1-mediated rounding of melanoma cells *in vivo* are not entirely clear at this time. Likewise, the actual activation patterns of Rac-1 and other GTPases in our system cannot be assessed. One may hypothesize, however, that smaller round cells may have advantages regarding extravasation, a notion that would be consistent with the long-known tumor-promoting activity of VCAM-1.

The α_4 integrin (CD49d, VLA-4) is involved in cell spreading and focal adhesion formation upon ligation (46,47). However, while the intracellular interaction of paxillin with dephosphorylated α_4 integrin and the downstream regulation of Rac-1 have been implicated in cellular morphogenesis (47–49), a plausible biophysical basis for the upstream VLA-4/VCAM-1 interaction on the ligand level has been lacking. We found that suppression of melanoma cell spreading on a “permissive” RGD matrix is most pronounced at a well-defined VCAM-1 site density of more than 280 ligands/μm^2 interspersed between RGD motifs. This bifunctional arrangement is a simplified model of an activated endothelium where VCAM-1 is highly expressed. It is conceivable, therefore, that VCAM-1 contains and controls the “permissive” environment created by RGD moieties on the respective surfaces. Considering that the regional, temporal and stimulus-specific parameters of VCAM-1 expression *in vivo* are still not fully understood, our tunable bifunctional *in vitro* model with a stoichiometrically defined presentation of VCAM-1 provides the first handle on the biophysical regulation of the VCAM-1/VLA-4 interaction on the nanoscale with respect to tumor cell morphogenesis. Furthermore, the formation of more mature paxillin-related adhesions (of ≈1 μm^2) on matrices with high densities of VCAM-1 (with VCAM-1 site distances in the range of 40 nm to 65 nm) might then be explained by dense clustering of its receptor, the VLA-4 integrin, on the melanoma cell side, which is predicted to physically facilitate the paxillin-VLA-4-interaction and subsequently inhibit cell spreading (47–49). It appears likely that the few large focal adhesions associated with high VCAM-1 densities mediated strong adhesion, while the smaller and more numerous focal adhesions together with the robust stress fiber formation seen on low VCAM-1 densities facilitated spreading of melanoma cells, thus providing a mechanistic explanation for the dichotomous function of VCAM-1. It is also in line with previous publications highlighting the relevance of VLA-4 for focal adhesion formation and melanoma cell motility (50–52).

In vivo, VCAM-1 is up-regulated through paracrine cytokine activation during melanoma progression. Therefore, it is conceivable that melanoma cells themselves modulate their micro-environment towards higher VCAM-1 densities. It is tempting to speculate that melanoma cells within the capillary beds benefit from the morphological changes effected by high densities of VCAM-1, e.g. through favored extravasation of smaller cells or improved intra-vascular immune escape of tumor cells with smaller surfaces. In concordance with this hypothesis, a recent study has shown that the ability of A375 melanoma cells to migrate in confined VCAM-1-coated microchannels depends on α_4/paxillin-mediated inhibition of Rac-1 activation (53). The dichotomic function of VCAM-1 identified here might thus facilitate two important steps of organ infiltration: first, firm interaction with the endothelium and second, morphological preparation for penetration within small niches in capillary beds. Mechanistically, down-regulation of Rac-1 has been identified as an important downstream event of enhanced VLA-4/paxillin interaction (53,54). Accordingly, we have detected a significant down-regulation of Rac-1 on high VCAM-1 densities, which is predicted to contribute to the inhibitory effect on melanoma cell spreading.

The regulation of VCAM-1 activity and its impact on tumor progression *in vivo* is not easy to fathom. In principle, regulation of endothelial VCAM-1 expression (modeled in our system by defined presentation at different densities) will in all likelihood influence tumor cell-endothelial cell interactions and modulate ”permissive” micro-environmental conditions for melanoma cells. However, the local VCAM-1 density, although up-regulated transcriptionally during inflammation, is also controlled through cleavage by leucocyte-derived proteases (27,28,55). As most, if not all, *in-vivo* studies showing a tumor-promoting function of VCAM-1 have been performed in models that include at least some degree of inflammation (18,23,41,56), it is difficult to gauge the regulation and net activity of VCAM-1 *in vivo*. We have, therefore, shown similar results in two complementary short-term mouse models, one without (untreated mice) and one with inflammation (MALP-2-treated mice with endothelial up-ragulation of VCAM-1 but concomitant influx of inflammatory cells). In any case, expression of VCAM-1 strong enough to be detectable by immunofluorescence microscopy appeared to suffice in our *in vivo* experiments to coerce melanoma cells into a globular shape at these micro-anatomical sites. In this light, nanotechnology provides a sophisticated tool to mimic, control and fine-tune the presentation of functionally active VCAM-1 on the physiologically relevant nanometer scale. It allowed for the first time to demonstrate that tuning VCAM-1 densities decisively regulates cytoskeletal and focal adhesion formation of human melanoma cells. In comparison to other ligands (e. g., RGD motifs (37) or cadherins, unpublished data), the dichotomic role for tumor cell adhesion on the one hand and spreading on the other, appears to be a rather unique feature of VCAM-1. Furthermore, it underlines the complexity of molecular interactions and implies a potential for unpredictable effects of blocking agents directed against VLA-4/VCAM-1 interactions. Finally, the bifunctional system with concomitant presentation of RGD shows that the remarkable capacity of VCAM-1 to modulate tumor cell spreading is relevant even when competing signals by “activating” integrins are involved.

Supplementary Material

Refer to Web version on PubMed Central for supplementary material.

Europe PMC Funders Author Manuscripts

Acknowledgments

We gratefully acknowledge the excellent technical assistance of K. Zachmann, S. Köchy and A. Bennemann and we thank Y. Schön and R. Koelz for the preparation of nanostructured matrices and subsequent quality control by scanning electron microscopy. J.P. Spatz is the Weston Visiting Professor at the Weizmann Institute of Science and part of the excellence cluster CellNetworks at the University of Heidelberg.

Financial support: J.P. Spatz acknowledges the financial support by the European Research Council under the European Union's Seventh Framework Programme (FP/2007-2013) / ERC Advanced Grant Agreement no. 294852.

References

1. Ott PA, Hodi FS, Robert C. CTLA-4 and PD-1/PD-L1 blockade: new immunotherapeutic modalities with durable clinical benefit in melanoma patients. Clin Cancer Res. 2013; 19:5300–5309. [PubMed: 24089443]
2. Robert C, Karaszewska B, Schachter J, Rutkowski P, Mackiewicz A, Stroiakovski D, Lichinitser M, Dummer R, Grange F, Mortier L, et al. Improved overall survival in melanoma with combined dabrafenib and trametinib. N Engl J Med. 2015; 372:30–39. [PubMed: 25399551]
3. Robert C, Long GV, Brady B, Dutriaux C, Maio M, Mortier L, Hassel JC, Rutkowski P, McNeil C, Kalinka-Warzocha E, et al. Nivolumab in previously untreated melanoma without BRAF mutation. N Engl J Med. 2015; 372:320–330. [PubMed: 25399552]
4. Hamid O, Robert C, Daud A, Hodi FS, Hwu WJ, Kefford R, Wolchok JD, Hersey P, Joseph RW, Weber JS, et al. Safety and tumor responses with lambrolizumab (anti-PD-1) in melanoma. N Engl J Med. 2013; 369:134–144. [PubMed: 23724846]
5. Wolchok JD, Kluger H, Callahan MK, Postow MA, Rizvi NA, Lesokhin AM, Segal NH, Ariyan CE, Gordon RA, Reed K, et al. Nivolumab plus ipilimumab in advanced melanoma. N Engl J Med. 2013; 369:122–133. [PubMed: 23724867]
6. Bald T, Quast T, Landsberg J, Rogava M, Glodde N, Lopez-Ramos D, Kohlmeyer J, Riesenberg S, van den Boorn-Konijnenberg D, Hömig-Hölzel C, et al. Ultraviolet-radiation-induced inflammation promotes angiotropism and metastasis in melanoma. Nature. 2014; 507:109–113. [PubMed: 24572365]
7. Wai Wong C, Dye DE, Coombe DR. The role of immunoglobulin superfamily cell adhesion molecules in cancer metastasis. Int J Cell Biol. 2012; 2012:340296. [PubMed: 22272201]
8. Läubli H, Borsig L. Selectins as mediators of lung metastasis. Cancer Microenviron. 2010; 3:97–105. [PubMed: 21209777]
9. Garofalo A, Chirivi RG, Foglieni C, Pigott R, Mortarini R, Martin-Padura I, Anichini A, Gearing AJ, Sanchez-Madrid F, Dejana E, et al. Involvement of the very late antigen 4 integrin on melanoma in interleukin 1-augmented experimental metastases. Cancer Res. 1995; 55:414–419. [PubMed: 7529137]
10. Martin-Padura I, Mortarini R, Lauri D, Bernasconi S, Sanchez-Madrid F, Parmiani G, Mantovani A, Anichini A, Dejana E. Heterogeneity in human melanoma cell adhesion to cytokine activated endothelial cells correlates with VLA-4 expression. Cancer Res. 1991; 51:2239–2241. [PubMed: 2009542]
11. Liang S, Dong C. Integrin VLA-4 enhances sialyl-Lewisx/a-negative melanoma adhesion to and extravasation through the endothelium under low flow conditions. Am J Physiol Cell Physiol. 2008; 295:C701–707. [PubMed: 18632734]
12. Okahara H, Yagita H, Miyake K, Okumura K. Involvement of very late activation antigen 4 (VLA-4) and vascular cell adhesion molecule 1 (VCAM-1) in tumor necrosis factor alpha enhancement of experimental metastasis. Cancer Res. 1994; 54:3233–3236. [PubMed: 7515767]
13. Rebhun RB, Cheng H, Gershenwald JE, Fan D, Fidler IJ, Langley RR. Constitutive expression of the alpha4 integrin correlates with tumorigenicity and lymph node metastasis of the B16 murine melanoma. Neoplasia. 2010; 12:173–182. [PubMed: 20126475]
14. Cardones AR, Murakami T, Hwang ST. CXCR4 enhances adhesion of B16 tumor cells to endothelial cells in vitro and in vivo via beta(1) integrin. Cancer Res. 2003; 63:6751–6757. [PubMed: 14583470]

15. HIgashiyama A, Watanabe H, Okumura K, Yagita H. Involvement of tumor necrosis factor alpha and very late activation antigen 4/vascular cell adhesion molecule 1 interaction in surgical-stress-enhanced experimental metastasis. Cancer Immunol Immunother. 1996; 42:231–236. [PubMed: 8665570]
16. Klemke M, Weschenfelder T, Konstandin MH, Samstag Y. High affinity interaction of integrin alpha4beta1 (VLA-4) and vascular cell adhesion molecule 1 (VCAM-1) enhances migration of human melanoma cells across activated endothelial cell layers. J Cell Physiol. 2007; 212:368–374. [PubMed: 17352405]
17. Schlesinger M, Bendas G. Vascular cell adhesion molecule-1 (VCAM-1)-An increasing insight into its role in tumorigenicity and metastasis. Int J Cancer. 2015; 136:2504–2514. [PubMed: 24771582]
18. Schill T, Schön MP, Pletz N, Emmert S, Schön M. Stimulation of pulmonary immune responses by the TLR2/6 agonist MALP-2 and effect on melanoma metastasis to the lung. Exp Dermatol. 2012; 21:91–98. [PubMed: 22044500]
19. Haddad O, Chotard-Ghodsnia R, Verdier C, Duperray A. Tumor cell/endothelial cell tight contact upregulates endothelial adhesion molecule expression mediated by NFkappaB: differential role of the shear stress. Exp Cell Res. 2010; 316:615–626. [PubMed: 19944683]
20. Chiu JJ, Chen LJ, Lee PL, Lee CI, Lo LW, Usami S, Chien S. Shear stress inhibits adhesion molecule expression in vascular endothelial cells induced by coculture with smooth muscle cells. Blood. 2003; 101:2667–2674. [PubMed: 12468429]
21. Chiu JJ, Lee PL, Chen CN, Lee CI, Chang SF, Chen LJ, Lien SC, Ko YC, Usami S, Chien S. Shear stress increases ICAM-1 and decreases VCAM-1 and E-selectin expressions induced by tumor necrosis factor-[alpha] in endothelial cells. Arterioscler Thromb Vasc Biol. 2004; 24:73–79. [PubMed: 14615388]
22. Partridge J, Carlsen H, Enesa K, Chaudhury H, Zakkar M, Luong L, Kinderlerer A, Johns M, Blomhoff R, Mason JC, et al. Laminar shear stress acts as a switch to regulate divergent functions of NF-kappaB in endothelial cells. Faseb J. 2007; 21:3553–3561. [PubMed: 17557931]
23. Strozyk EA, Desch A, Poeppelmann B, Magnolo N, Wegener J, Huck V, Schneider SW. Melanoma-derived IL-1 converts vascular endothelium to a proinflammatory and procoagulatory phenotype via NFkappaB activation. Exp Dermatol. 2014; 23:670–676. [PubMed: 25041487]
24. Langley RR, Carlisle R, Ma L, Specian RD, Gerritsen ME, Granger DN. Endothelial expression of vascular cell adhesion molecule-1 correlates with metastatic pattern in spontaneous melanoma. Microcirculation. 2001; 8:335–345. [PubMed: 11687945]
25. Läubli H, Spanaus KS, Borsig L. Selectin-mediated activation of endothelial cells induces expression of CCL5 and promotes metastasis through recruitment of monocytes. Blood. 2009; 114:4583–4591. [PubMed: 19779041]
26. Simiantonaki N, Jayasinghe C, Kirkpatrick CJ. Effect of pro-inflammatory stimuli on tumor cell-mediated induction of endothelial cell adhesion molecules in vitro. Exp Mol Pathol. 2002; 73:46–53. [PubMed: 12127053]
27. Garton KJ, Gough PJ, Philalay J, Wille PT, Blobel CP, Whitehead RH, Dempsey PJ, Raines EW. Stimulated shedding of vascular cell adhesion molecule 1 (VCAM-1) is mediated by tumor necrosis factor-alpha-converting enzyme (ADAM 17). J Biol Chem. 2003; 278:37459–37464. [PubMed: 12878595]
28. Levesque JP, Takamatsu Y, Nilsson SK, Haylock DN, Simmons PJ. Vascular cell adhesion molecule-1 (CD106) is cleaved by neutrophil proteases in the bone marrow following hematopoietic progenitor cell mobilization by granulocyte colony-stimulating factor. Blood. 2001; 98:1289–1297. [PubMed: 11520773]
29. Pletz N, Schön M, Ziegelbauer K, Emmert S, Liu N, Dobbelstein M, Schön MP. Exp Dermatol. 2012; 21:301–4. [PubMed: 22320445]
30. Lohmüller T, Aydin D, Schwieder M, Morhard C, Louban I, Pacholski C, Spatz JP. Nanopatterning by block copolymer micelle nanolithography and bioinspired applications. Biointerphases. 2011; 6:MR1–12. [PubMed: 21428688]

Europe PMC Funders Author Manuscripts

31. Kruss S, Erpenbeck L, Schön MP, Spatz JP. Circular, nanostructured and biofunctionalized hydrogel microchannels for dynamic cell adhesion studies. Lab Chip. 2012; 12:3285–3289. [PubMed: 22858992]
32. Glass R, Möller M, Spatz JP. Block copolymer micelle nanolithography. Nanotechnology. 2003; 14:1153–1160.
33. Kruss S, Erpenbeck L, Amschler K, Mundinger TA, Boehm H, Helms HJ, Friede T, Andrews RK, Schön MP, Spatz JP. Adhesion maturation of neutrophils on nanoscopically presented platelet glycoprotein Ibα. ACS Nano. 2013; 7:9984–9996. [PubMed: 24093566]
34. Kuo JC, Han X, Hsiao CT, Yates JR 3rd, Waterman CM. Analysis of the myosin-II-responsive focal adhesion proteome reveals a role for beta-Pix in negative regulation of focal adhesion maturation. Nat Cell Biol. 2011; 13:383–393. [PubMed: 21423176]
35. Ranzinger J, Krippner-Heidenreich A, Haraszi T, Bock E, Tepperink J, Spatz JP, Scheurich P. Nanoscale arrangement of apoptotic ligands reveals a demand for a minimal lateral distance for efficient death receptor activation. Nano Lett. 2009; 9:4240–4245. [PubMed: 19772290]
36. Wolfram T, Belz F, Schoen T, Spatz JP. Site-specific presentation of single recombinant proteins in defined nanoarrays. Biointerphases. 2007; 2:44–48. [PubMed: 20408635]
37. Amschler K, Erpenbeck L, Kruss S, Schön MP. Nanoscale integrin ligand patterns determine melanoma cell behavior. ACS Nano. 2014; 8:9113–9125. [PubMed: 25171587]
38. Koo LY, Irvine DJ, Mayes AM, Lauffenburger DA, Griffith LG. Co-regulation of cell adhesion by nanoscale RGD organization and mechanical stimulus. J Cell Sci. 2002; 115:1423–1433. [PubMed: 11896190]
39. Chua GL, Patra AT, Tan SM, Bhattacharjya S. NMR structure of integrin alpha4 cytosolic tail and its interactions with paxillin. PLoS One. 2013; 8:e55184. [PubMed: 23383101]
40. Parri M, Chiarugi P. Rac and Rho GTPases in cancer cell motility control. Cell Commun Signal. 2010; 8:23. [PubMed: 20822528]
41. Petrocelli T, Slingerland J. UVB induced cell cycle checkpoints in an early stage human melanoma line, WM35. Oncogene. 2000; 19:4480–4490. [PubMed: 11002421]
42. Taranova AG, Maldonado D 3rd, Vachon CM, Jacobsen EA, Abdala-Valencia H, McGarry MP, Ochkur SI, Protheroe CA, Doyle A, Grant CS, et al. Allergic pulmonary inflammation promotes the recruitment of circulating tumor cells to the lung. Cancer Res. 2008; 68:8582–8589. [PubMed: 18922934]
43. Soto MS, Serres S, Anthony DC, Sibson NR. Functional role of endothelial adhesion molecules in the early stages of brain metastasis. Neuro Oncol. 2014; 16:540–551. [PubMed: 24311639]
44. Vidal-Vanaclocha F, Fantuzzi G, Mendoza L, Fuentes AM, Anasagasti MJ, Martín J, Carrascal T, Walsh P, Reznikov LL, Kim SH, et al. IL-18 regulates IL-1beta-dependent hepatic melanoma metastasis via vascular cell adhesion molecule-1. Proc Natl Acad Sci U S A. 2000; 97:734–739. [PubMed: 10639148]
45. Kienast Y, von Baumgarten L, Fuhrmann M, Klinkert WE, Goldbrunner R, Herms J, Winkler F. Real-time imaging reveals the single steps of brain metastasis formation. Nat Med. 2010; 16:116–122. [PubMed: 20023634]
46. Kassner PD, Alon R, Springer TA, Hemler ME. Specialized functional properties of the integrin alpha 4 cytoplasmic domain. Mol Biol Cell. 1995; 6:661–674. [PubMed: 7579686]
47. Liu S, Thomas SM, Woodside DG, Rose DM, Kiosses WB, Pfaff M, Ginsberg MH. Binding of paxillin to alpha4 integrins modifies integrin-dependent biological responses. Nature. 1999; 402:676–681. [PubMed: 10604475]
48. Deakin NO, Bass MD, Warwood S, Schoelermann J, Mostafavi-Pour Z, Knight D, Ballestrem C, Humphries MJ. An integrin-alpha4-14-3-3zeta-paxillin ternary complex mediates localised Cdc42 activity and accelerates cell migration. J Cell Sci. 2009; 122:1654–1664. [PubMed: 19401330]
49. Han J, Liu S, Rose DM, Schlaepfer DD, McDonald H, Ginsberg MH. Phosphorylation of the integrin alpha 4 cytoplasmic domain regulates paxillin binding. J Biol Chem. 2001; 276:40903–40909. [PubMed: 11533025]
50. Iida J, Meijne AM, Spiro RC, Roos E, Furcht LT, McCarthy JB. Spreading and focal contact formation of human melanoma cells in response to the stimulation of both melanoma-associated

proteoglycan (NG2) and alpha 4 beta 1 integrin. Cancer Res. 1995; 55:2177–2185. [PubMed: 7743521]

51. Mostafavi-Pour Z, Askari JA, Parkinson SJ, Parker PJ, Ng TT, Humphries MJ. Integrin-specific signaling pathways controlling focal adhesion formation and cell migration. J Cell Biol. 2003; 161:155–167. [PubMed: 12695503]
52. Moyano JV, Maqueda A, Casanova B, Garcia-Pardo A. Alpha4beta1 integrin/ligand interaction inhibits alpha5beta1-induced stress fibers and focal adhesions via down-regulation of RhoA and induces melanoma cell migration. Mol Biol Cell. 2003; 14:3699–3715. [PubMed: 12972558]
53. Hung WC, Chen SH, Paul CD, Stroka KM, Lo YC, Yang JT, Konstantopoulos K. Distinct signaling mechanisms regulate migration in unconfined versus confined spaces. J Cell Biol. 2013; 202:807–824. [PubMed: 23979717]
54. Nishiya N, Kiosses WB, Han J, Ginsberg MH. An alpha4 integrin-paxillin-Arf-GAP complex restricts Rac activation to the leading edge of migrating cells. Nat Cell Biol. 2005; 7:343–352. [PubMed: 15793570]
55. Garton KJ, Gough PJ, Raines EW. Emerging roles for ectodomain shedding in the regulation of inflammatory responses. J Leukoc Biol. 2006; 79:1105–1116. [PubMed: 16565325]
56. Salado C, Olaso E, Gallot N, Valcarcel M, Egilegor E, Mendoza L, Vidal-Vanaclocha F. Resveratrol prevents inflammation-dependent hepatic melanoma metastasis by inhibiting the secretion and effects of interleukin-18. J Transl Med. 2011; 9:59. [PubMed: 21569399]

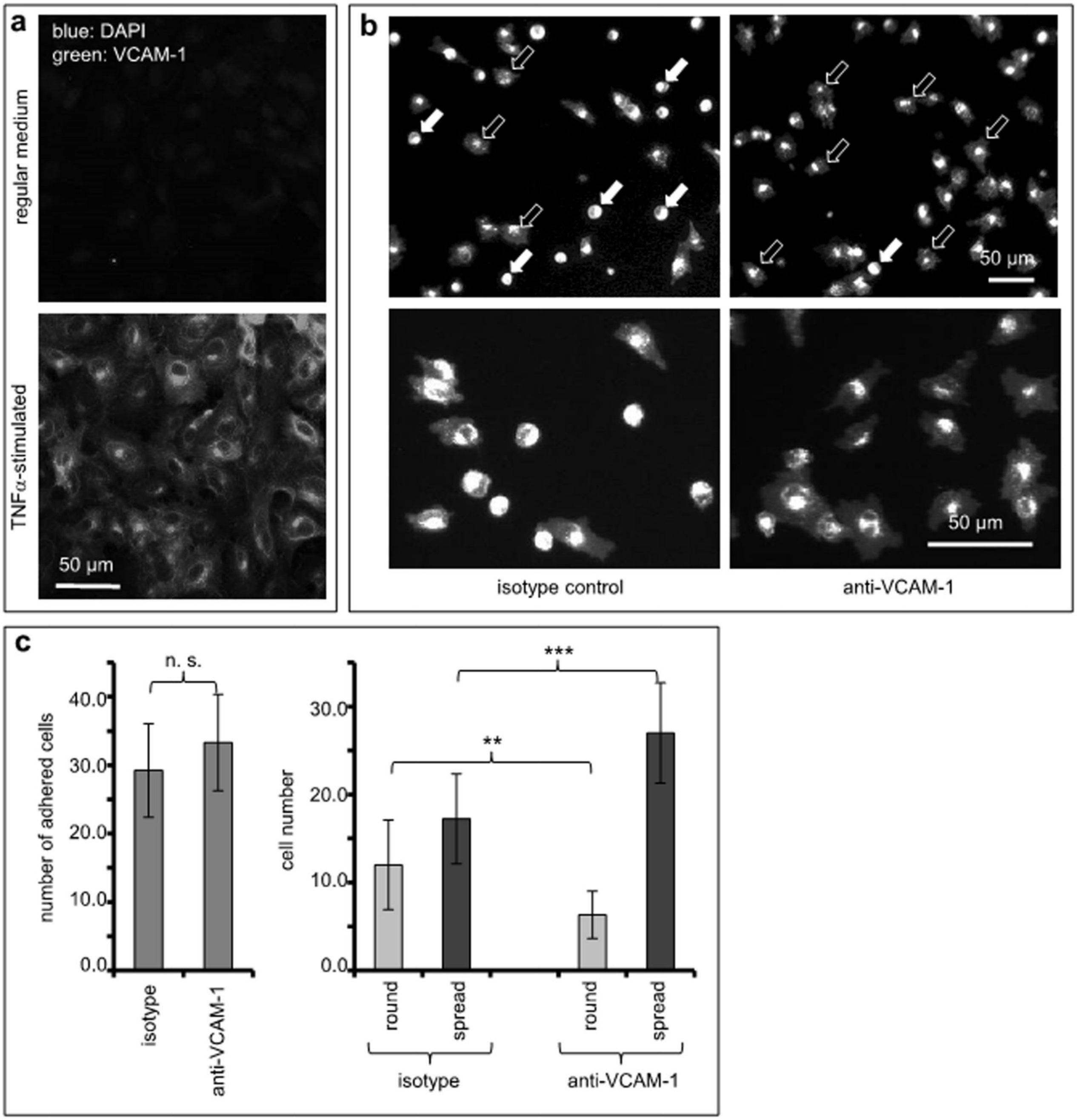

Figure 1. VCAM-1 inhibition facilitates melanoma cell spreading on endothelial cells.
(**a**) Human endothelial cells were cultured without (top panel) or in the presence of TNFα (25 ng/ml, bottom panel) to stimulate expression of adhesion molecules. Expression of VCAM-1 was visualized by immunofluorescence. (**b**) Human endothelial cells stimulated with TNFα and expressing VCAM-1 were treated with an isotype-matched control antibody (left photomicrographs) or with a function-blocking antibody directed against VCAM-1 (right photomicrographs). Human melanoma cells (A375) fluorescently labeled with PKH26 were allowed to adhere for 40 min to these endothelial cell cultures. Images depict low (top

panels) and high magnification (bottom panels), respectively. In the upper two photomicrographs, filled arrows indicate examples of round, non-spread melanoma cells, and open arrows indicate examples of spread melanoma cells. (**c**) The total numbers of melanoma cells adhered to TNF-stimulated endothelial cell cultures were quantitated (left graph). In addition, the numbers of non-spread (round) and spread melanoma cells, respectively, were quantitated separately both on endothelial cells treated with isotype-matched and VCAM-directed antibodies (right graph). The values shown represent averages from 12 random microscopic fields for each condition. The experiment was repeated twice. **indicates $p<0.01$, ***indicates $p<0.001$.

Europe PMC Funders Author Manuscripts

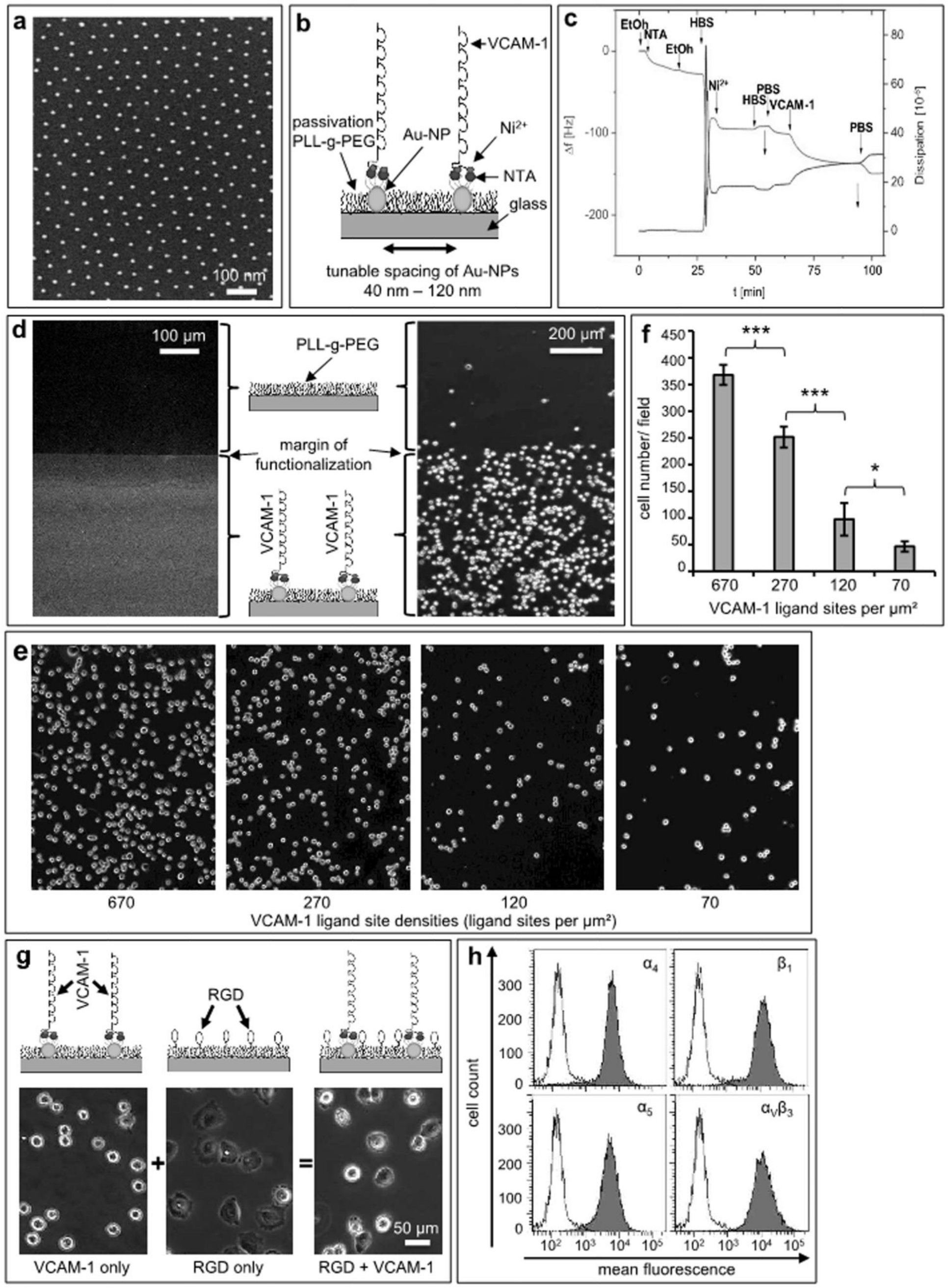

Figure 2. Nanoscopic presentation of VCAM-1 facilitates attachment and diminishes spreading of human melanoma cells.

(**a**) Representative scanning electron microscopy (SEM) image of gold nanopatterns (Au-NPs) on glass (d=98 ±11nm). (**b**) Schematic of biofunctionalization: *Via* its C-terminal 6His tag, VCAM-1 is immobilized in a site-directed manner to NTA-groups bound on gold nanoparticles (Au-NPs). (**c**) The subsequent steps of biofunctionalization on gold were monitored by Quartz Crystal Microbalance with Dissipation (QCMD) measurements. The frequency/dissipation changes show successful conjugation of the VCAM-1-molecule. (**d**)

Immunofluorescence image of the border-region between nanostructured and non-nanostructured areas using a fluorescent antibody directed against VCAM-1, which creates a sharply demarcated line (margin of functionalization; left photomicrograph). The clear contrast indicates immobilization of VCAM-1 on the Au-NPs and shows a low nonspecific background. The right hand phase contrast image again depicts the margin of functionalization and demonstrates that A375-melanoma cells adhere almost exclusively to the side functionalized with VCAM-1 nanopatterns but not to the pegylation side. (**e**) Defined gold nanoparticle matrices were bio-functionalized with VCAM-1 yielding ligand presentations at the indicated densities. The spaces between the ligand sites were passivated by (PLL-g-PEG) without RGD. Human melanoma cells adhered to these matrices for 45 min, and the matrices were then washed in a standardized fashion. (**f**) Melanoma cells which had firmly adhered to the matrices depicted in (e) were quantitated microscopically. The values shown represent mean numbers from 10 standardized microscopic fields (SD). *indicates $p<0.05$, and *** indicates $p<0.001$. The experiment was repeated with similar results. (**g**) Matrices with nanoscopically defined VCAM-1 (left), RGD motifs in-between the passivating pegylation (middle) or both (right, bifunctional matrix) were generated as detailed in Material and Methods. Representative phase-contrast photomicrographs of A375-melanoma cells on nanoscopic-VCAM-1 (65 nm) after a washing-step with PBS for 10 minutes showing attachment but no spreading on nanoscopic VCAM-1 (left, upper panel), full spreading when RGD motifs are interspersed within the pegylation (middle panel) and reduced spreading when nanosopic VCAM-1 and RGD are combined in a bifunctional matrix (right), respectively. (**h**) Flow cytometry histograms depicting the melanoma cell expression of integrins relevant for binding to RGD ($\alpha_5\beta_1$, $\alpha_V\beta_3$) or VCAM-1 ($\alpha_4\beta_1$).

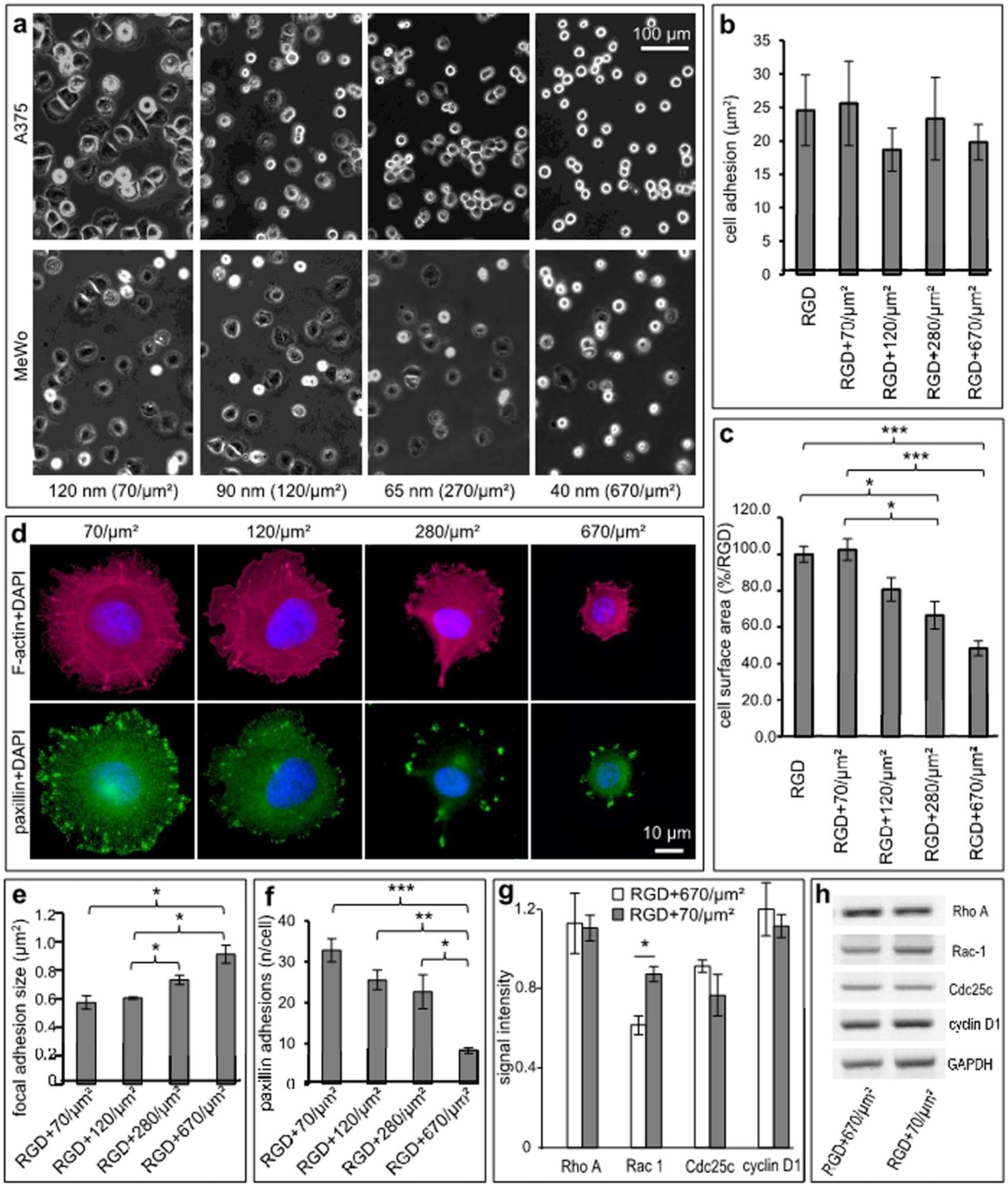

Figure 3. VCAM-1 density determines melanoma cell plasticity.

(**a**) Representative phase-contrast photomicrographs of A375 (upper row) and MeWo (lower row) melanoma cells interacting with bifunctional matrices (RGD + VCAM-1) with increasing site densities of VCAM-1 (ligand site distances of 120, 90, 65 and 40 nm, respectively, corresponding to ligand site densities ranging from 70/µm^2 to 670/µm^2 VCAM-1-ligands). (**b**) A375-melanoma cells showing similar quantitative attachment independent of variations of VCAM-1 density (by one order of magnitude) next to RGD. (**c**) Cell spreading as determined by measuring of the cell surface areas is reduced on matrices with high densities of VCAM-1 indicating an inverse linear correlation of cell surface and VCAM-1 density. Analysis of A375-melanoma cells was performed after 1 h and cell spreading on the control matrices (RGD alone) was set to 100%. Relative to this control, tunable nanoscopic presentation significantly inhibits cell spreading in a density-dependent manner. Values shown represent the mean (± SEM) of 6 independent experiments. (p=0.0001 for RGD control vs. 670/μm^2 (ligand distance: 40 nm), p=0.0243 for RGD control vs. 280/μm^2 (ligand distance: 65 nm), p=0.0005 for 70/μm^2 (ligand distance: 120 nm) vs. 670/μm^2 (ligand distance: 65 nm), p=0.0440 for 70/μm^2 (ligand distance: 120 nm) vs. 280/μm^2 (ligand distance: 65 nm); global effect between 40, 65, 90 and 120 nm, respectively, was assessed using one way ANOVA, pairs were then analyzed with the two-sided Student's t-test and subsequent Bonferroni-adjustment. *P<0.05, ***P<0.001). (**d**) Anti-paxillin and phalloidin were used to stain focal adhesions (green) and F-actin fibers (red), respectively. VCAM-1-densities of 70 sites per μm^2 (ligand distances of 120 nm) and 120 sites per μm^2 (distances of 90 nm), respectively, support stress fiber formation in contrast to ligand site densities ≥ 280/μm^2 (distances ≤ 65 nm) (upper panel). Size and number of paxillin adhesions are regulated by VCAM-1-density (lower panel). (**e**) Statistical evaluation showing mean focal adhesion sizes of melanoma cells bound to VCAM-1 at the indicated site densities within a pegylated surface interspersed with RGD. Paxillin adhesions ranging from 0.1 to 5 μm^2 were regarded as focal adhesions and analyzed morphometrically. The average size of paxillin adhesions directly correlates with increased VCAM-1 density. Values shown represent the mean (± SEM) of 4 independent experiments (p = 0.0201 for 70/μm^2 vs. 670/μm^2, p = 0.0111 for 120/μm^2 vs. 670/μm^2 and p = 0.0371 for 120/μm^2 vs. 280/μm^2, *P<0.05; analyzed with the two-sided Student's t-test). (**f**) The number of focal adhesions (0.1 – 5 μm^2) per melanoma cell bound to VCAM-1 at the indicated site densities next to RGD. The number of paxillin adhesions shows an inverse linear correlation with the densities of VCAM-1. Values shown represent the mean (± SEM) of 4 independent experiments. (p=0.0005 for 70/μm^2 vs. 670/μm^2, p = 0.0013 for 120/μm^2 vs. 670/μm^2 and p = 0.0441 for 280/μm^2 vs. 670/μm^2. For all statistical analysis, unpaired Bonferroni adjusted t-tests were used. * p < 0.05, ** p < 0.01, *** p < 0.001). (**g**) A375-melanoma cells were incubated on bifunctional matrices (RGD + VCAM-1 at the indicated site densities) for 3 hours prior to analyzing expression of RhoA, Rac-1, Cdc25 and Cyclin D1 using RT-PCR. Relative expression was determined using GAPDH for normalization. Values shown represent the mean of 3 independent experiments. (p=0.0130 for Rac-1 expression on 670 ligand sites per μm^2 vs. on 70 ligand sites per μm^2). (**h**) Human melanoma cells (A375) were incubated on bifunctional matrices (RGD + VCAM-1 at the indicated site densities) for 3 hours prior to analyzing gene expression by RT-PCR. The panels depict the results of a representative experiment (out of three experiments showing similar results). Only Rac-1 is expressed at higher levels on low-density VCAM-1 compared to high-density VCAM-1.

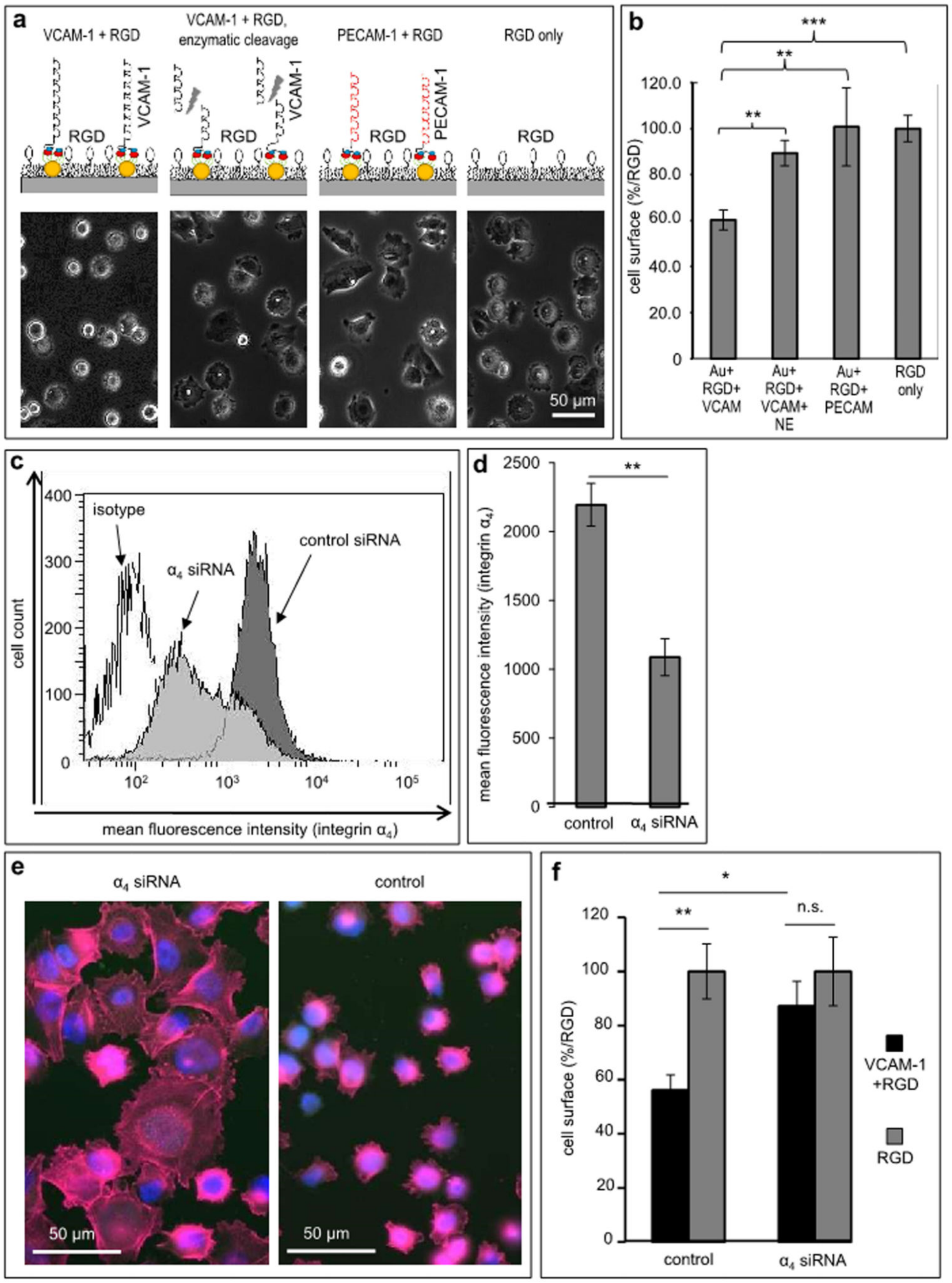

Figure 4. Melanoma cell plasticity is regulated specifically by VCAM-1/VLA-4.

(a) Specificity controls for the functional effect of VCAM-1 with regard to the inhibition of RGD-induced cell spreading were performed by modification of VCAM-1 presentation, which is depicted schematically in the upper panels (presentation of intact VCAM-1, left; enzymatic cleavage of VCAM-1 by neutrophil elastase, second from left; replacement of VCAM-1 with PECAM-1, third from left; RGD-only matrices, right). All experiments were performed on VCAM-1 ligand site distances of 65 nm. The lower panels depict representative photomicrographs from each of the indicated matrices showing that only intact VCAM-1 can inhibit RGD-induced melanoma cell spreading. (**b**) Melanoma cells adhered to the matriced specified in (a) for 60 min. The cell surface area was determined under each condition. Values shown represent the mean (± SEM) of 3 independent experiments (≥100 cells were analyzed per matrix/condition; $p=0.0076$ for VCAM-1 vs. truncated VCAM-1, $p=0.0040$ for VCAM-1 vs. PECAM-1 and $p=0.0001$ for VCAM-1 vs. RGD control. ** $p<0.01$, *** $p<0.001$, analyzed with the two-sided Student's t-test). (**c**) Human A375 melanoma cells were subjected to down-regulation of the α_4 integrin subunit by siRNA. The histograms depict a representative flow cytometry experiment showing integrin VLA-4 expression after treatment with control siRNA (dark grey curve), α_4-directed siRNA (light grey curve) and an isotype control (open curve). (**d**) An average reduction of 50% in α_4-expression was achieved by transfection of A375 melanoma cells with α_4-directed siRNA compared to control siRNA, respectively. Values shown represent the mean (±SEM) of 4 independent experiments (** $p<0.01$, analyzed with the two-sided Student's t-test.) (**e**) Melanoma cells transfected with α_4-directed siRNA are able to spread on a RGD-containing matrix with nanoscopic VCAM-1 (left photomicrograph). In contrast, melanoma cells treated with control siRNA are inhibited in cell spreading on nanoscopic VCAM-1 (right photomicrograph). The phalloidin/DAPI fluorescence image shows impaired F-actin filament organization. (**f**) Statistical evaluation of cell spreading: Melanoma cells treated with control-siRNA are clearly inhibited in cell spreading compared to melanoma cells treated with α4-siRNA on nanoscopic VCAM-1 within a RGD-containing matrix (black bars, relative to the respective RGD controls). Both subpopulations (control vs. α_4-knock-down cells) are able to spread on the RGD control (light grey bars). Values shown represent the mean (±SEM) of 3 independent experiments. ($p=0.0278$ for control siRNA transfected cells vs. α4 siRNA knock down cells, $p=0.0092$ for control siRNA transfected melanoma cells on RGD+VCAM-1 vs. RGD-only presentation, Student's two-tailed, unpaired t-test).

Europe PMC Funders Author Manuscripts

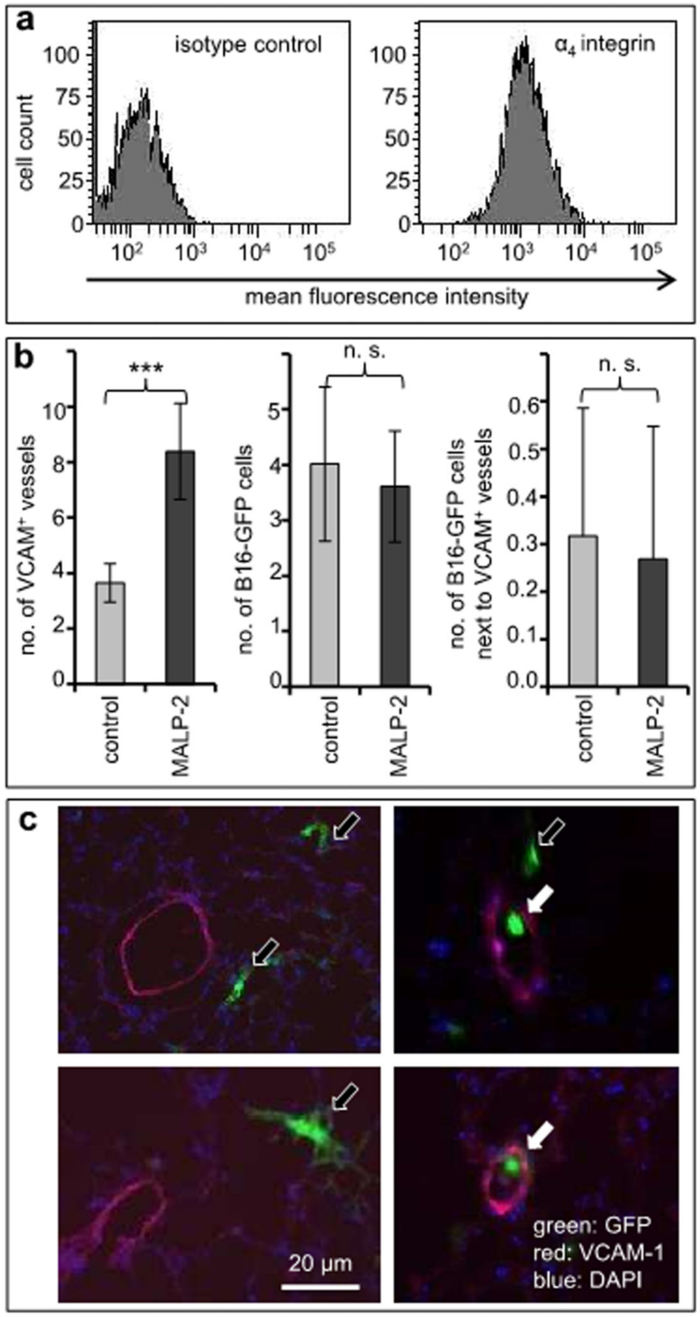

Figure 5. Pulmonary VCAM-1 expression *in vivo* is associated with morphogenesis of melanoma cells.

(**a**) Murine B16F10 melanoma cells stably transfected with GFP were analyzed for expression of VLA-4, the ligand of VCAM-1, by flow cytometry. (**b**) C57BL6 mice were left untreated (light gray bars) or treated by intra-tracheal instillation of MALP-2. After 24 h. the mice were injected intravenously with 10^6 GFP-labeled B16F10 melanoma cells. The lungs of the mice were harvested after 1, 5 or 30 min (n=3 mice per group) and snap-frozen in liquid nitrogen. GFP-labeled melanoma cells as well as VCAM-1-expressing pulmonary blood vessels were analyzed in cryostat-cut sections by fluorescence microscopy. The left graph depicts the average numbers of VCAM-1-expressing pulmonary blood vessels indicating induction by MALP-2. The middle and the right graphs depict the total numbers of melanoma cells and melanoma cells adjacent to VCAM-1-expressing blood vessels, respectively. Values shown represent mean counts from 41 microscopic fields (±SD). ***indicates $p<0.001$. (**c**) Representative examples of cryostat-cut sections showing areas with GFP-expressing melanoma cells (green) adjacent to (filled arrows) or distant from (open arrows) VCAM-1-expressing pulmonary blood vessels (red).

Europe PMC Funders Author Manuscripts

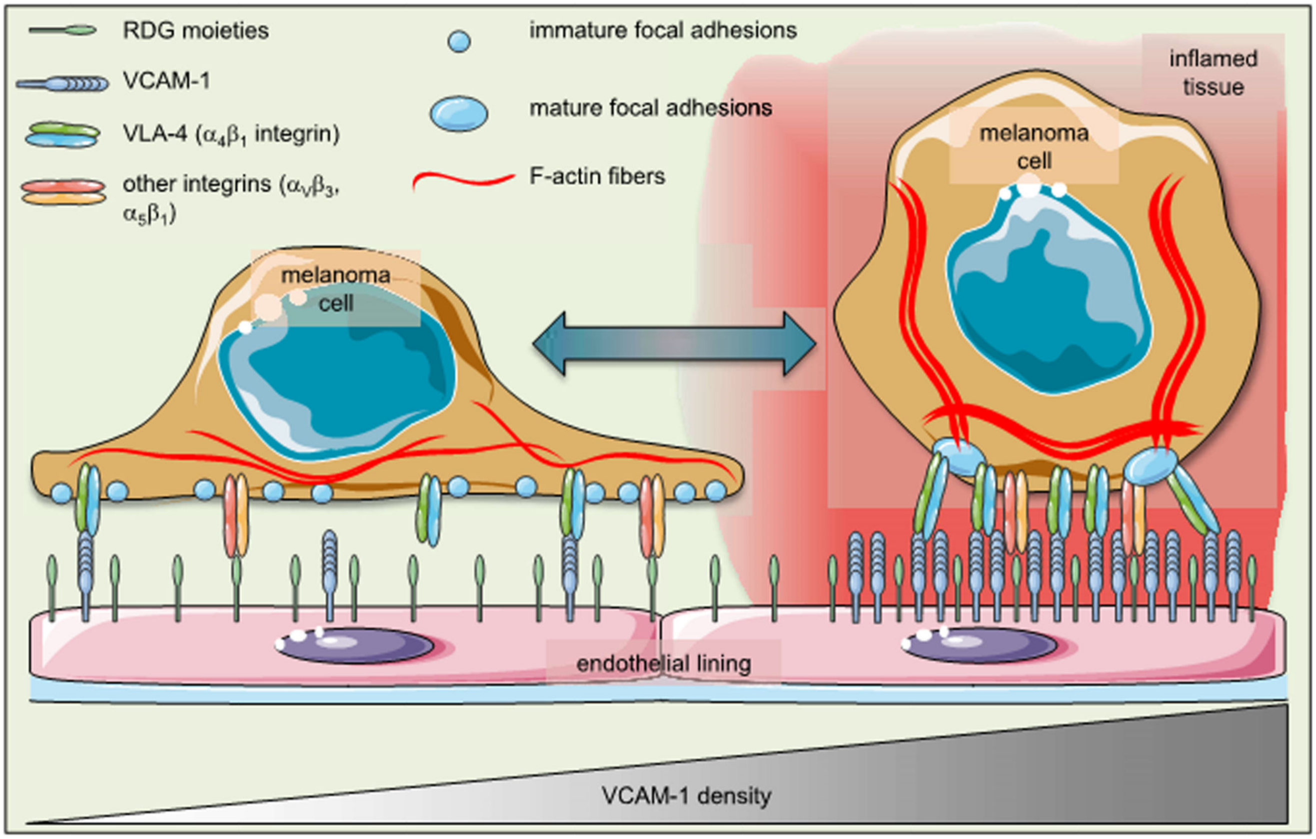

Figure 6. Endothelial VCAM-1 tips the balance in melanoma cell plasticity.

The schematic illustrates the cellular consequences following modulation of the VCAM-1 density in a putative (micro)environment that is permissive for cell spreading. At low densities of VCAM-1, RGD moieties facilitate spreading of melanoma cells. This morphological phenotype is also characterized by numerous immature focal adhesions and delicate F-actin fibers. High densities of VCAM-1, in contrast, force the cell into a globular shape with fewer but mature focal adhesions and prominent F-actin stress fibers. This “morphogenic dictate” of VCAM-1 overrules the still-present signals by RGD moieties.